



Published in final edited form as:

*Cell Metab.* 2005 May ; 1(5): 343–354.

## Differential regulation of TRPM channels governs electrolyte homeostasis in the *C. elegans* intestine

Takayuki Teramoto<sup>1</sup>, Eric J. Lambie<sup>2</sup>, and Kouichi Iwasaki<sup>1,\*</sup>

<sup>1</sup> Northwestern University Medical School, Institute for Neuroscience, Department of Molecular Pharmacology and Biological Chemistry, 303 E. Chicago Avenue, Searle 5-551, Chicago, Illinois 60611

<sup>2</sup> Department of Biological Sciences, Dartmouth College, Hanover, New Hampshire 03755

### Summary

The transient receptor potential (TRP) channels are implicated in various cellular processes, including sensory signal transduction and electrolyte homeostasis. We show here that the GTL-1 and GON-2 TRPM channels regulate electrolyte homeostasis in the *C. elegans* intestine. GON-2 is responsible for a large outwardly rectifying current of intestinal cells, and its activity is tightly regulated by intracellular Mg<sup>2+</sup> levels, while GTL-1 mainly contributes to appropriate Mg<sup>2+</sup> responsiveness of the outwardly rectifying current. We also used nickel cytotoxicity to study the function of these channels. Both GON-2 and GTL-1 are necessary for intestinal uptake of nickel, but GTL-1 is continuously active while GON-2 is inactivated at higher Mg<sup>2+</sup> levels. This type of differential regulation of intestinal electrolyte absorption ensures a constant supply of electrolytes through GTL-1, while occasional bursts of GON-2 activity allow rapid return to normal electrolyte concentrations following physiological perturbations.

### Introduction

Magnesium (Mg<sup>2+</sup>) is one of the most abundant cations in the human body and is involved in more than 300 enzymatic systems, including adenosine triphosphate (ATP) metabolism (Fox et al., 2001). Hypomagnesemia has been identified in 7% of general clinical patients, 24% of hypertensive patients, and 25% of diabetic patients (Fox et al., 2001). Low-level Mg<sup>2+</sup> deficiency is typically asymptomatic, but severe Mg<sup>2+</sup> deficiency causes a variety of symptoms, including impaired memory, cardiac rhythm disturbances, and seizures (Vormann, 2003). In spite of the biological and clinical importance of the Mg<sup>2+</sup> ion, little is known about the mechanism of its homeostatic regulation.

It has been speculated that Mg<sup>2+</sup> uptake in eukaryotic cells is mainly mediated by transporters (Romani and Scarpa, 2000). This is partly because Mg<sup>2+</sup> transporters have been cloned in prokaryotic cells and partly because the antiporter that extrudes Mg<sup>2+</sup> in exchange for extracellular Na<sup>+</sup> was identified in vertebrate cells (Romani and Scarpa, 2000). However, no firm evidence has been provided supporting the importance of transporters in eukaryotic Mg<sup>2+</sup> homeostasis (Wolf, 2004).

Recent studies have implied that the transient receptor potential (TRP) channels are involved in regulation of Mg<sup>2+</sup> homeostasis in eukaryotes (Clapham, 2003). TRP channel proteins are classified into seven subfamilies based on amino acid sequences (TRPC, TRPV, TRPM, TRPA, TRPN, TRPP, and TRPML) and are implicated in a range of physiological processes (Birnbaumer et al., 2003; Clapham, 2003; Minke and Cook, 2002; Montell, 2001; Montell,

\*Correspondence: k-iwasaki@northwestern.edu.

2003b). Mutations in TRPM6 result in familial hypomagnesemia with secondary hypocalcemia (HSH), an autosomal recessive disease caused by a defect in intestinal  $Mg^{2+}$  absorption (Schlingmann et al., 2002; Walder et al., 2002). The related channel TRPM7 has also been implicated in  $Mg^{2+}$  homeostasis. TRPM7-deleted cell lines are not viable in the absence of  $Mg^{2+}$  in the culture medium, but they are viable when the medium is supplemented with a high level of  $Mg^{2+}$  (Schmitz et al., 2003). TRPM6 and TRPM7 both are characterized by the presence of a protein kinase domain in the C-terminal cytoplasmic domain (Nadler et al., 2001; Runnels et al., 2001; Schlingmann et al., 2002; Walder et al., 2002), and their channel activities are regulated by millimolar levels of intracellular  $Mg^{2+}$  (Nadler et al., 2001; Runnels et al., 2001; Schmitz et al., 2003; Voets et al., 2004). These observations imply that TRPM6 and TRPM7 channels are involved in the regulation of vertebrate  $Mg^{2+}$  homeostasis (Montell, 2003a).

We have investigated intestinal  $Mg^{2+}$  homeostasis using the model organism *C. elegans*. The *C. elegans* intestine is a tube composed of ten pairs of epithelial cells arrayed along its length (White, 1987). A dense layer of microvilli is present on the apical (luminal) side of each intestinal cell, and these microvilli are presumably involved in the secretion of digestive enzymes and the absorption of nutrients and ions (White, 1987). The intestinal cells are attached to each other by adherens junctions at the borders of the apical membrane (White, 1987). In vertebrates, two pathways for electrolyte absorption by epithelial cells have been proposed, transcellular and paracellular (Aronson et al., 2003). The transcellular pathway is mediated by ion channels and transporters, whereas the paracellular pathway involved the “loosening” of tight junctions between epithelial cells. No reports have previously addressed the importance of either of these two pathways in the absorption of electrolytes by the *C. elegans* intestine.

Here we describe our investigation of the function of the *C. elegans* TRPM channels GTL-1 and GON-2. The *gon-2; gtl-1*-double mutants show growth defects under low  $Mg^{2+}$  conditions, and these defects can be largely rescued by dietary supplementation with excess  $Mg^{2+}$ . GTL-1 and GON-2 are also necessary for intestinal  $Ni^{2+}$  uptake since *gtl-1; gon-2*-double mutants become resistant to  $Ni^{2+}$  cytotoxicity. *gtl-1* mutants are resistant to  $Ni^{2+}$ , but this resistance is dependent on the presence of  $Mg^{2+}$  in the medium. This suggests that GON-2-dependent  $Ni^{2+}$  transport is tightly regulated by  $Mg^{2+}$  levels but GTL-1-dependent  $Ni^{2+}$  transport is not. Using a  $Ni^{2+}$ -sensitive fluorescence indicator, we found that the wild-type intestine incorporates  $Ni^{2+}$  from the environment, but the double mutant intestine does so to a lesser extent. Finally, our electrophysiological data show that the large outwardly rectifying current characteristic of wild-type intestinal cells is mainly due to the activity of the GON-2 channel and that GON-2 and GTL-1 play different roles in the  $Mg^{2+}$  sensitivity of current generation. These observations suggest that two TRPM channels with different degrees of  $Mg^{2+}$  responsiveness are necessary to regulate appropriate intestinal electrolyte homeostasis and that this type of differential regulation of intestinal electrolyte absorption ensures a constant supply of electrolytes through GTL-1, while occasional bursts of GON-2 activity allow rapid return to normal electrolyte concentrations following physiological perturbations.

## Results

### Molecular and genetic characterization of the *gtl-1* TRPM gene

The *C. elegans* genome encodes four TRPM family members, GON-2, GTL-1, GTL-2, and CED-11 (Harteneck et al., 2000). CED-11 is very distant from the three other TRPM proteins, but the remaining TRPM proteins are similar to one another. The overall amino acid identities of these channels between human and *C. elegans* are modest (21%–26%), but the N-terminal cytoplasmic domains are more closely related (Figure 1 and see Figures S1 and S2 in the Supplemental Data available with this article online). Our structural comparison suggests that the *C. elegans* TRPM channels resemble human TRPM1, 3, 6, and 7 within the TRPM

subfamily (Figure 1A). However, the C termini of these TRPM channels are diverse. For example, TRPM6 and TRPM7 contain a kinase domain, which is absent from the *C. elegans* TRPM channels.

To examine which cells express these TRPM channels, we made fusion genes between GFP and the promoters of *gon-2*, *gtl-1*, and *gtl-2*. In transgenic animals, *Pgon-2s(9)::gfp* and *Pgtl-1(7)::gfp* were strongly expressed in the intestine while *Pgtl-2(12)::gfp* was predominantly expressed in the excretory cell (Figure 1B). In addition to *Pgtl-1(7)::gfp*, we also investigated the expression patterns of different *gtl-1::gfp* constructs and found that all of these were expressed in the intestine (Figure S3). We also found that a full-length fusion between *gtl-1* and GFP was expressed throughout the intestine, with accumulation at the apical surface toward the intestinal lumen (Figure S3). Previously, two different 5' ends of the *gon-2* transcript were described (one starts at nt 20643 and the other at nt 9278 of cosmid T01H8) (West et al., 2001). Here we found that GFP fluorescence was strongly expressed in the intestine when we used the potential promoter region containing the initiation site for the shorter transcript (the promoter for the longer transcript expressed GFP in other cell types; Figure S4).

Since mutations in human TRPM6 have been reported to cause hypomagnesemia with secondary hypocalcemia (HSH) due to insufficient intestinal  $Mg^{2+}$  absorption (Schlingmann et al., 2002; Walder et al., 2002), we decided to use genetic analysis to determine whether GON-2 and/or GTL-1 mediate  $Mg^{2+}$  uptake in the *C. elegans* intestine. Recessive loss-of-function mutations in *gon-2* were previously isolated based on their sterile phenotype (Sun and Lambie, 1997), but there was no indication that *gon-2* functions in the intestine. No functional characterization of *gtl-1* has been previously reported. Therefore, we isolated the deletion allele *gtl-1(tg113)* by trimethyl-psoralen/UV mutagenesis combined with PCR-based screening (Figure 1C). Another *gtl-1* deletion allele (*ok375*) was isolated by the *C. elegans* Genome Knockout Consortium (<http://www.wormbase.org/>). *tg113* is a deletion of 328 nucleotides within the fifth exon, resulting in a frame shift that truncates the protein coding sequence. The *ok375* deletion is 2714 bp in size, and this deletes all GTL-1 transmembrane domains (Figure 1C). Therefore, *tg113* and *ok375* are both expected to strongly reduce or eliminate *gtl-1* activity.

### The *gon-2;gtl-1* double mutant is suppressible by $Mg^{2+}$ supplementation

On standard NGM plates, which contain 1 mM  $CaCl_2$  and 1 mM  $MgSO_4$  (Epstein and Shakes, 1995), the *gtl-1* mutants showed no obvious abnormal phenotypes. However, we found that, when these mutants were placed on culture plates containing 0 mM  $Mg^{2+}$ , they grew much slower than wild-type (Figure 2A). In fact, some animals arrested before reaching adulthood. It should be noted that a small amount of  $Mg^{2+}$  is present even in the 0 mM  $Mg^{2+}$  plates, and this is unavoidable because *E. coli* as a food source carries trace amounts of the ions. As expected based on previous results (Sun and Lambie, 1997), growth of the *gon-2* mutant was not much affected by different levels of  $Mg^{2+}$  supplementation (Figure 2A).

Since *gon-2* and *gtl-1* are both expressed in the intestine, we suspected that they might function redundantly in this tissue. Therefore, we constructed double mutant strains to investigate this possibility. Strikingly, the *gon-2;gtl-1*-double mutants showed a severe growth phenotype (Figure 2A). The double mutants did not reach adulthood at all when low  $Mg^{2+}$  was present in the culture agar. On 5 mM  $Mg^{2+}$  plates, 11%–35% of the double mutants reached adulthood, but it took them two to three times longer than wild-type (Figure 2A). On higher  $Mg^{2+}$  plates, nearly 100% of the double mutants reached adulthood 120 hr after hatching (Figure 2A).

To test whether or not the altered growth rates on different  $Mg^{2+}$  concentrations were simply due to differences in osmolarity, we placed these strains on culture plates that contained 80 mM sucrose but no supplemental  $Mg^{2+}$ . Mutants grown on sucrose behaved similarly to ones

on 0 mM  $Mg^{2+}$  plates (Figure 2A), indicating that the effect of  $Mg^{2+}$  on growth rate is not simply osmotic in nature.

We further investigated the effects of  $Mg^{2+}$  and/or  $Ca^{2+}$  depletion on mutant growth by adding 5 mM EDTA and EGTA: no  $Mg^{2+}$  or  $Ca^{2+}$  was added to the medium, but it is likely that the *E. coli* provided as a food source carried in trace amounts of these ions. In the presence of 5 mM EDTA in the culture agar, none of the animals reached adulthood (Figure 2B), instead arresting around the L2 stage. When 5 mM EGTA was present in the medium, wild-type and *gon-2* animals showed a near-normal growth phenotype (Figure 2B). Only 70%–80% of the *gtl-1* mutants reached adulthood, and none of the *gon-2;gtl-1*-double mutants grew to adulthood (Figure 2B). Furthermore, we found that  $Mg^{2+}$  supplementation rescued the growth arrest of the *gtl-1*-single and *gon-2;gtl-1*-double mutants, even in the presence of 5 mM EGTA (Figure 2B). We also found that high-dose  $Mg^{2+}$  supplementation relieves the  $Mg^{2+}$  deficiency phenotypes in the single and double mutants, even after they temporarily arrested in the absence of  $Mg^{2+}$  (Figure S5). Taken together, these observations indicate that  $Mg^{2+}$  deficiency is the primary cause of the phenotypes of the *gtl-1*-single and *gon-2;gtl-1*-double mutants.

We also tested whether  $Ca^{2+}$  in the culture media would affect the *gon-2* and *gtl-1* phenotypes. We found that  $Ca^{2+}$  supplementation had little effect on the growth of the mutant strains, with the exception of the *gtl-1* mutants (Figure 2C). Excess  $Ca^{2+}$  in the culture medium slowed down the growth of the *gtl-1* mutants, and some of these animals ruptured at the vulva. Since TRPM7 is implicated in incorporating  $Ca^{2+}$  for neural cell death (Nicotera and Bano, 2003), one possible explanation for this result is that, when GTL-1 is not active, GON-2 might transport excess  $Ca^{2+}$  into the intestine (and possibly other tissues), leading to necrosis (also see Figures 6 and 7).

### ***gon-2; gtl-1*-double mutants contain less $Mg^{2+}$ than wild-type**

To determine whether  $Mg^{2+}$  deficiency is observed in the *gon-2; gtl-1*-double mutant, we quantitated the amounts of trace elements in the wild-type and double mutant animals using inductively coupled plasma mass spectrometry (ICP-MS). We found that wild-type contained 1850 ppm  $Mg^{2+}$  (standard error  $\pm 80$ ), while the double mutant contained only 1020 ppm  $Mg^{2+}$  ( $\pm 80$ ;  $p < 0.05$ ; trial = 4). No significant difference was detected in the quantities of other elements, including  $Ca^{2+}$  and  $K^+$ , between these strains. This result is also consistent with the notion that the phenotypes in the *gon-2;gtl-1*-double mutants were indeed caused by  $Mg^{2+}$  deficiency.

### **Characterization of the defecation behavior in the *gon-2* and *gtl-1* mutants**

In order to investigate the physiological state of the intestine, we examined the defecation motor program (DMP) cycles. The *C. elegans* defecation behavior is regulated by the activity of the inositol 1,4,5-trisphosphate receptor (IP3R) (Dal Santo et al., 1999). The DMP consists of a stereotyped series of three muscle contractions (Figure 3) (Liu and Thomas, 1994; Thomas, 1990). First, posterior body wall muscles contract (pBoc) and then relax, causing the gut contents to accumulate near the anus. Three to four seconds later, the anterior body wall muscles contract (aBoc) to pressurize the gut contents. Finally, specialized enteric muscles contract to expel the contents from the anus (Exp). This defecation motor program is expressed as a periodic behavior: in the presence of abundant food, the defecation motor program is activated every 45 s (Figure 3) (Liu and Thomas, 1994; Thomas, 1990).

Wild-type animals showed DMP cycles of 40–45 s on both 40 mM and 0 mM  $Mg^{2+}$  plates. Therefore, their defecation cycles were not obviously affected by different  $Mg^{2+}$  concentrations. This suggests that the wild-type intestine can maintain normal physiological levels of intracellular  $Mg^{2+}$  over a wide range of environmental  $Mg^{2+}$  concentrations (Figure

3B). On 40 mM Mg<sup>2+</sup> plates, *gtl-1* mutants showed a mean cycle of 40 s, which is very close to wild-type (Figure 3B). The cycles of both *gtl-1* mutants were highly variable on 0 mM Mg<sup>2+</sup> plates. Forty percent of the *gtl-1* mutants still exhibited DMP cycles around 45 s, but 60% of the mutants had much longer DMP cycles (80–200 s; Figure 3A). Therefore, intestinal activity was severely attenuated in the majority of *gtl-1* mutants grown on 0 mM Mg<sup>2+</sup> plates.

The *gon-2* mutant showed slightly slower DMP cycles than wild-type on both 40 mM and 0 mM Mg<sup>2+</sup> plates (around 60 s), suggesting that the DMP phenotype in the *gon-2* mutant is not due to insufficient Mg<sup>2+</sup> (Figure 3B). Interestingly, the DMP phenotype of the double mutant on 40 mM Mg<sup>2+</sup> was near normal, indicating that the *gtl-1* mutations are epistatic to *gon-2* (*q388*) (Figure 3B).

Although no detectable phenotypes were observed in the growth rate of the *gon-2* mutant in response to excess Ca<sup>2+</sup> supplementation, the DMP of the *gon-2* mutant was partially suppressed by supplementation with 5 mM Ca<sup>2+</sup>. Since the *gtl-1*-single mutant is not suppressible by Ca<sup>2+</sup> supplementation, this implies that GON-2 and GTL-1 play different roles in regulating the physiological state of the intestine (Figure 3B).

To assess the DMP phenotype of *gon-2;gtl-1*-double mutants under low Mg<sup>2+</sup> conditions, these animals were raised on 40 mM Mg<sup>2+</sup> plates until the L3 larval stage and then transferred to 0 mM Mg<sup>2+</sup> plates (Figure 3B). Twenty-four hours after transfer onto 0 mM Mg<sup>2+</sup> plates, the double mutants showed very sluggish DMPs (Figure 3B). When these animals were transferred back to 40 mM Mg<sup>2+</sup> plates, their DMP cycles returned to near normal (Figure 3B). These observations suggest that the altered DMP cycle in the double mutant is due to an alteration in the physiological state of the intestine, rather than a developmental defect. These results also suggest that the observed impairment of the DMP cycle is mainly caused by Mg<sup>2+</sup> deficiency. A similar plate transfer assay using 40 mM Ca<sup>2+</sup> supplementation at the second transfer did not rescue the DMP cycles (Figure 3B). Although we cannot completely eliminate the possibility that Ca<sup>2+</sup> signaling is also altered in the double mutants, the most parsimonious explanation is that Mg<sup>2+</sup> acts directly to rescue the mutant phenotypes.

As with the growth assays, we found that the *gtl-1* and *gon-2*-single mutants do not have overlapping phenotypes, whereas the double mutant exhibits a more severe phenotype. Therefore, our data suggest that GTL-1 and GON-2 function independently, with overlapping functions, to regulate physiology of the intestinal cells.

### Ni<sup>2+</sup> toxicity assays reveal differential regulation of GON-2 and GTL-1 activity by Mg<sup>2+</sup> levels

TRPM7 has been reported to permeate trace divalent ions, such as Ni<sup>2+</sup>, Zn<sup>2+</sup>, Fe<sup>2+</sup>, Cu<sup>2+</sup>, Mn<sup>2+</sup>, and Co<sup>2+</sup> (Monteilh-Zoller et al., 2003), in addition to Mg<sup>2+</sup> and Ca<sup>2+</sup>, as originally reported (Nadler et al., 2001). These divalent ions are required as cofactors for many essential enzymes, and some of them, such as Ni<sup>2+</sup>, cause cellular toxicity at relatively low concentrations (Monteilh-Zoller et al., 2003). Also, it has been shown that TRPM6 can pass Ni<sup>2+</sup> as well (Voets et al., 2004). Therefore, we hypothesized that, if either GTL-1 or GON-2 can pass these trace divalent ions, then mutations in these genes might confer resistance to toxicity. We chose Ni<sup>2+</sup> for this assay for two reasons. First, Ni<sup>2+</sup> is already known to cause cellular toxicity in *C. elegans*, so we could easily establish an assay to detect Ni<sup>2+</sup> resistance (Peredney and Williams, 2000). Second, fluorescence indicators are commercially available that are sensitive to Ni<sup>2+</sup>, thus making it possible to monitor absorption of Ni<sup>2+</sup> by living intestinal cells (Cabantchik et al., 1996; Jussofie et al., 1998).

We began by testing the Ni<sup>2+</sup> sensitivity of each strain on 40 mM Mg<sup>2+</sup> plates, since all strains could grow at this Mg<sup>2+</sup> concentration (Figure 4). Little or no effect was seen among any of the strains when the concentration of Ni<sup>2+</sup> was lower than 0.2 mM (Figure 4A). However, on



0.5 mM Ni<sup>2+</sup> plates containing 40 mM Mg<sup>2+</sup>, both wild-type and *gon-2* mutant animals arrested at L1 to L2 stages (Figure 4A). This is in contrast to the *gon-2;gtl-1*-double mutants, which grew unaffected even with 0.5 mM Ni<sup>2+</sup>, suggesting that a lack of these channels confers Ni<sup>2+</sup> resistance (Figure 4A). However, at 1 mM Ni<sup>2+</sup>, the double mutants arrested as early larvae (data not shown). This suggests that the double mutants are able to take up Ni<sup>2+</sup>, but they do so less efficiently than wild-type. The *gtl-1*-single mutants showed an intermediate level of resistance to Ni<sup>2+</sup>: at 0.5 mM Ni<sup>2+</sup>, nearly 50% of them became adults, and these animals looked unhealthy (Figure 4A). These observations indicate that GTL-1 and GON-2 are able to function independently to mediate Ni<sup>2+</sup> uptake and that GTL-1 activity is primarily responsible for Ni<sup>2+</sup> uptake under these assay conditions.

On 0 mM Mg<sup>2+</sup> plates, both wild-type and *gon-2* mutant animals had growth rates similar to those observed on 40 mM Mg<sup>2+</sup> plates: at increasing Ni<sup>2+</sup> concentrations, fewer animals reached adulthood (Figure 4A). Interestingly, *gtl-1* mutants were sensitive to Ni<sup>2+</sup> (0.2 and 0.5 mM) when raised on 0 mM Mg<sup>2+</sup> plates. Therefore, the Ni<sup>2+</sup> resistance of *gtl-1* mutants depends on the Mg<sup>2+</sup> concentration. The *gon-2;gtl-1*-double mutants did not grow at all, but this is because of Mg<sup>2+</sup> deficiency, not Ni<sup>2+</sup> toxicity (see Figure 2). Although the double mutants did not progress developmentally on 0.5 mM Ni<sup>2+</sup> 0 mM Mg<sup>2+</sup> plates, these animals moved vigorously and looked healthy, whereas wild-type incubated on such plates barely moved and looked very unhealthy. To quantitate the viability of the double mutants on the 0 mM Mg<sup>2+</sup> plates, we performed a thrashing assay, counting the number of times per minute the animal swung from side to side when suspended in a saline solution. In the presence of 0 mM Mg<sup>2+</sup> and 0.5 mM Ni<sup>2+</sup>, the double mutants thrashed vigorously, much more so than wild-type (Figure 4B). Nearly all wild-type animals died after 120 hr of incubation with 0.5 mM Ni<sup>2+</sup>, but the double mutants stayed alive for up to 192 hr. At lower Ni<sup>2+</sup> levels, the wild-type and double mutants were equally viable (Figure 4B). These observations suggest that the double mutants are still resistant to 0.5 mM Ni<sup>2+</sup> even with 0 mM Mg<sup>2+</sup>.

To complete this set of experiments, we tested the effects of low-level Mg<sup>2+</sup> supplementation. On 1 mM Mg<sup>2+</sup> plates, both wild-type and *gon-2* mutant animals showed growth rates similar to those on 0 mM and 40 mM Mg<sup>2+</sup> plates (Figure 4A). This confirms the idea that the Ni<sup>2+</sup> sensitivity of these strains is not greatly affected by Mg<sup>2+</sup> concentration. However, the growth rates of the *gtl-1* mutants were intermediate between those observed on 0 and 40 mM Mg<sup>2+</sup> plates (Figure 4A). These observations indicate that the *gtl-1* mutants become more resistant to Ni<sup>2+</sup> as Mg<sup>2+</sup> concentration increases. On the other hand, the *gon-2* mutant was sensitive to Ni<sup>2+</sup> even at 40 mM Mg<sup>2+</sup>.

To test whether Ni<sup>2+</sup> is absorbed through intestinal cells, we measured Ni<sup>2+</sup> uptake in dissected intestines. Intestinal explants were loaded with 20 μM calcein AM in dissection solution for 30 min at room temperature. Calcein shows fluorescence quenching upon Ni<sup>2+</sup> binding (Cabantchik et al., 1996). Therefore, Ni<sup>2+</sup> uptake by intestinal cells is signaled by a decrease in calcein fluorescence. We used the maximum slope of fluorescence quenching to quantitate the rate of Ni<sup>2+</sup> absorption by the most anterior intestinal cells (Figure 5). When Ni<sup>2+</sup> concentration was increased stepwise from 0.01 mM to 0.1 mM and then 1 mM, the quenching rate became progressively larger, 0.8%, 1.8%, and 4.7%/minute, respectively (Figure 5A, n = 3 each).

To test whether GTL-1 and GON-2 are responsible for Ni<sup>2+</sup> uptake, intestines were loaded with calcein and perfused with a solution containing 1 mM NiCl<sub>2</sub>, after which nonspecific fluorescence quenching rates were measured. We performed this assay using animals that were grown on both 40 mM Mg<sup>2+</sup> plates and standard NGM plates and found consistent results: the double mutant absorbed Ni<sup>2+</sup> much slower than wild-type (Figure 5). However, we detected no significant difference in Ni<sup>2+</sup> uptake among wild-type, *gtl-1*-single, and *gon-2*-single

mutants (Figure 5). These results are consistent with the notion that both GTL-1 and GON-2 are important for the uptake of  $\text{Ni}^{2+}$  by the intestine.

### Outwardly rectifying currents are diminished in the mutants of *gon-2*

To test whether any electrophysiological properties were altered in the intestinal cells of these TRPM mutants, we attempted electrophysiological analysis of the intestinal cells derived from *C. elegans* embryos using the method of Estevez et al. (2003). Intestinal cells in culture were identifiable based on their distinct round morphology and autofluorescent granules (Estevez et al., 2003). In wild-type, we observed an outwardly rectifying current using the whole-cell configuration (its reversal potential  $[E_{\text{rev}}] = -3.7 \pm 6.4$  mV), and this current appears to be voltage modulated, which is also observed with TRPM4b and TRPM5 (Hofmann et al., 2003). This current was suppressed by 0.1 mM  $\text{LaCl}_3$  in the bath solution (Figure 6). When we measured the electrophysiological activities of *gtl-1* mutant cells, we found that the current was very similar to that of wild-type cells (Figure 6), suggesting that contribution of the GTL-1 channel to the amplitude of this current is small. In the *gon-2* mutant cells, the outwardly rectifying current was severely attenuated; at 80 mV, we observed a current of  $15.8 \pm 3.5$  pA/pF without  $\text{LaCl}_3$  (at 80 mV, the current was  $30.5 \pm 6.1$  pA/pF in the wild-type), suggesting that this outwardly rectifying current is mainly generated by GON-2 (Figure 6). In the case of the *gon-2(q388);gtl-1(ok375)* double mutant cells, the current was small as well. We did not observe further reduction of the current amplitude compared to that of the *gon-2* mutant cells (Figure 6). These observations indicated that GON-2 is mainly responsible for this outwardly rectifying current and that contribution of GTL-1 to the current amplitude is very small.

To study the selectivity of the GON-2-dependent conductance, we replaced the  $\text{Na}^+$  solution with solutions containing only one of the cations  $\text{NMDG}^+$ ,  $\text{Ca}^{2+}$ ,  $\text{Mg}^{2+}$ , or  $\text{Ni}^{2+}$  (Figure 6). When 120 mM  $\text{Ca}^{2+}$  was exchanged for 150 mM  $\text{Na}^+$ , the  $E_{\text{rev}}$  shift was  $+45.9 \pm 7.9$  mV ( $n = 5$ ). When 120 mM  $\text{Mg}^{2+}$  was exchanged for  $\text{Na}^+$ , the shift was  $-4.5 \pm 2.8$  mV ( $n = 5$ ).  $\text{NMDG}^+$  was used as a nonpermeable cation for this conductance; the  $E_{\text{rev}}$  shift between  $\text{Na}^+$  and  $\text{NMDG}^+$  solutions was  $-67.4 \pm 6.8$  mV ( $n = 14$ ) ( $P_{\text{NMDG}^+}/P_{\text{Na}^+} = 0.06$ ). These results indicate that  $\text{Ca}^{2+}$  is more permeable than  $\text{Mg}^{2+}$ , which is nearly as permeable as  $\text{Na}^+$ . When we tried to measure the  $\text{Ni}^{2+}$  permeability for the current, we found that 120 mM  $\text{Ni}^{2+}$  completely blocked the inward current (data not shown). When we lowered the  $\text{Ni}^{2+}$  concentration to 5 mM, we found that  $\text{Ni}^{2+}$  was significantly more permeable than  $\text{NMDG}^+$ ; the  $E_{\text{rev}}$  difference between  $\text{Ni}^{2+}$  and  $\text{NMDG}^+$  was  $14.2 \pm 4.3$  mV ( $n = 5$ ,  $p < 0.05$ ). These results show that the GON-2-dependent current can conduct  $\text{Ni}^{2+}$  in addition to  $\text{Ca}^{2+}$  and  $\text{Mg}^{2+}$ .

To examine the effect of intracellular  $\text{Mg}^{2+}$  concentration on the activity of the GON-2-dependent current, cells were patch clamped with an ATP- and GTP-free pipette solution in which EGTA was replaced by 10 mM BAPTA. The concentration of  $\text{MgCl}_2$  added to the pipette solution varied between 0 mM and 6 mM. In wild-type, the current amplitude was gradually suppressed when  $\text{Mg}^{2+}$  levels added in the pipette solution were increased from 0 mM to 6 mM (Figure 7). In the *gtl-1* mutant cells, as in wild-type, the current amplitude was reduced upon intracellular  $\text{Mg}^{2+}$  increase. However, the reduction in current from 0 mM to 1 mM  $\text{Mg}^{2+}$  was steeper than in the wild-type cells (Figure 7). In the *gon-2* mutant cells, no significant difference was observed in the current amplitude when 0, 1, and 3 mM  $\text{Mg}^{2+}$  were added in the pipette solution, but a significant decrease occurred between 3 mM and 6 mM  $\text{Mg}^{2+}$  ( $p < 0.05$ ,  $n = 5$  and 8) (Figure 7). In the case of the *gon-2(q388);gtl-1(ok375)* double mutant cells, no significant difference in current amplitude was observed among different  $\text{Mg}^{2+}$  levels (Figure 7).

To further investigate the role of GTL-1, we compared the effects of intracellular  $\text{Mg}^{2+}$  concentration on the outwardly rectifying current in wild-type and *gtl-1(ok375)* mutant cells

(Figure 7). Currents were recorded by stepping from a holding voltage of 0 mV to voltages between  $-100$  and  $+100$  mV in 20 mV intervals, and then the amplitudes of steady-state current at  $+80$  mV were normalized based on the mean amplitude at  $+80$  mV of 0 mM  $Mg^{2+}$  added in the pipette solution. In wild-type cells, we observed a gradual decrease in the current amplitude as an intracellular free  $Mg^{2+}$  concentration was increased (Figure 7). However, in *gtl-1* mutant cells, the amplitude was sharply reduced in response to a slight increase in free  $Mg^{2+}$  (Figure 7). The estimated  $K_{1/2}$  values of free  $Mg^{2+}$  were  $186 \mu M$  for the *gtl-1* mutant and  $874 \mu M$  for wild-type ( $n = 3-7$  of each point/strain). These electrophysiological data support the notion that GTL-1 channel is responsible for appropriate  $Mg^{2+}$  sensitivity.

## Discussion

In this paper, we describe our characterization of the function of the GTL-1 and GON-2 channels in *C. elegans*. Our results show that these channels regulate  $Mg^{2+}$  homeostasis in the *C. elegans* intestine. Single mutations in either *gtl-1* or *gon-2* cause little or no defect in defecation or overall growth rate; however, *gon-2;gtl-1*-double mutants exhibit strong synthetic phenotypes, and these are efficiently suppressed by  $Mg^{2+}$  supplementation. We have also found that the GON-2 and GTL-1 channels are necessary for  $Ni^{2+}$  uptake in the intestine, and the results of these assays indicate that these channels have different sensitivities to  $Mg^{2+}$  levels. Finally, we have obtained electrophysiological data that support the idea that the GON-2 channel is mainly responsible for the outwardly rectifying current and that GON-2 and GTL-1 play different roles in the  $Mg^{2+}$  sensitivity of current generation. Overall, our findings indicate that *C. elegans* provides an appropriate animal model to study intestinal electrolyte homeostasis mediated by TRPM channels.

### Independent functioning of the GON-2 and GTL-1 TRPM channels

It has been reported that mammalian TRPM6 and TRPM7 form heteromeric channels (Chubanov et al., 2004). Our data indicate that formation of GON-2/GTL-1 heteromers is not essential for cellular function in the *C. elegans* intestine under laboratory conditions. The *gtl-1* and *gon-2* single mutants show distinct phenotypes with respect to growth, defecation,  $Ni^{2+}$  resistance, and EDTA-induced arrest. If heteromer formation were essential for their function, a lack of either channel should have induced some overlapping phenotypes between the *gtl-1* and *gon-2* single mutants. On the contrary, no overlapping behavioral or overall growth phenotypes were observed between these single mutants. Furthermore, the *gon-2;gtl-1* double mutants showed strong synthetic phenotypes that were not observed with either single mutant, suggesting that these channels function independently and have overlapping functions. When one channel species is absent, the other channel can compensate for the function of the missing channel species to some extent but not completely. Therefore, based on these genetic data, we conclude that, while heteromers may exist, they are unlikely to perform any major unique or essential function under the laboratory conditions we used.

### TRP channels and $Mg^{2+}$ homeostasis

Estevez et al. (2003) previously identified two major conductances in cultured *C. elegans* intestinal cells: an outwardly rectifying current (named  $I_{ORCa}$ ) and an inwardly rectifying current ( $I_{SOC}$ ).  $I_{ORCa}$  is 60 times more permeable to  $Ca^{2+}$  than  $Na^{+}$ , and it is suppressed by both extracellular  $La^{3+}$  and intercellular  $Mg^{2+}$ . Although we used the same conditions as Estevez et al. (2003) to measure the outwardly rectifying current, we cannot be certain that the outwardly rectifying current that we measured is equivalent to  $I_{ORCa}$ . For example, when we measured conductance in  $Na^{+}$  solution containing 1 mM EDTA, we still observed strong outward rectification, whereas  $I_{ORCa}$  was reported to exhibit a more linear voltage-current relation under these conditions, particularly at positive voltage (Estevez et al., 2003).



Our electrophysiological recordings suggest that GON-2-dependent current is  $\text{Ca}^{2+}$  selective, although this current can conduct other cations and poorly discriminate between  $\text{Na}^{+}$  and  $\text{Mg}^{2+}$ . Since mammalian TRPM6 and TRPM7 also show permeability to various ions in addition to  $\text{Mg}^{2+}$  under physiological conditions, it is likely that  $\text{Mg}^{2+}$  homeostasis is tightly linked with homeostasis of other electrolytes, including  $\text{Ca}^{2+}$ .

Our electrophysiological data support the idea that the GON-2 channel is mainly responsible for the outwardly rectifying current and that GON-2 and GTL-1 play different roles in  $\text{Mg}^{2+}$  sensitivity. This difference in  $\text{Mg}^{2+}$  sensitivity is also consistent with the differences in  $\text{Ni}^{2+}$  toxicity observed with the *gtl-1* and *gon-2* mutants (Figure 4). The GON-2 channel appears to be inactive in the range between 0 and 1 mM  $\text{Mg}^{2+}$ . However, the GTL-1 channel is probably little inhibited by cytoplasmic  $\text{Mg}^{2+}$  because the *gon-2* mutant was sensitive to  $\text{Ni}^{2+}$  toxicity even with a high  $\text{Mg}^{2+}$  level. In this sense, GTL-1 might have properties similar to other TRPMs, such as TRPM3, the activity of which is not inhibited by even 5 mM  $\text{Mg}^{2+}$  (Grimm et al., 2003). In general, cytosolic levels of free  $\text{Mg}^{2+}$  are believed to range from 0.2 mM to 1 mM, and this concentration is tightly regulated (Flatman, 1991). If this is also applicable to the *C. elegans* intestinal cells, then we would expect that GTL-1 is constitutively active, whereas GON-2 would exhibit strong feedback inhibition in response to increased levels of intracellular  $\text{Mg}^{2+}$ . This type of inverse correlation between current amplitudes and  $\text{Mg}^{2+}$ -dependent negative feedback could be important in the regulation of intestinal physiology. GON-2 can probably pass a larger quantity of different ion species in a short time in order to compensate for physiological deviations from the normal state. However, such a lack of ion selectivity would also render GON-2 activity susceptible to producing side effects such as acute metal cytotoxicity. Therefore, GON-2 activity would need to be tightly regulated by a feedback mechanism coupled with monitoring the physiological state or, in this case, detection of intracellular  $\text{Mg}^{2+}$  levels. On the other hand, GTL-1 can be active continuously, because it mediates only a low level of electrolyte uptake. But this property of GTL-1 would render cells susceptible to chronic toxicity, as found with  $\text{Ni}^{2+}$  (Figure 4). This type of differential regulation of intestinal electrolyte absorption probably ensures a constant supply of electrolytes through GTL-1, while occasional bursts of GON-2 activity allow rapid return to normal electrolyte concentrations following physiological perturbations. Our findings show that GON-2 and GTL-1 TRPM channels regulate intestinal electrolyte homeostasis in *C. elegans* and that TRPM channels are responsible for intestinal  $\text{Mg}^{2+}$  uptake.

## Experimental procedures

### Genetics

Methods for *C. elegans* culture and genetic analysis were as previously described (Epstein and Shakes, 1995). A deletion within the *gtl-1* locus (*tg113*) was isolated by using PCR to screen the knockout library generated by H. Inada and I. Mori (personal communication). Screening was performed as described previously (Jansen et al., 1997). *gtl-1(ok375)* was isolated by the *C. elegans* gene knockout consortium (<http://www.wormbase.org/>). The construction of the *gon-2; gtl-1 IV* double mutants are described in Supplemental Data.

### Phenotypic assays

Growth assays were performed as follows. All strains were maintained on NGM plates containing 40 mM  $\text{MgSO}_4$  and 0 mM  $\text{CaCl}_2$  for at least three generations at 20°C. Eggs from each strain were first transferred to 0 mM  $\text{Mg}^{2+}$  0 mM  $\text{Ca}^{2+}$  plates and then transferred to each assay plate (50 eggs/plate) as described in the figure legends. Then, all strains were grown at 25°C in parallel and the number of adults was counted every 12 hr. Adults of the *gon-2* (*q388*) and the *gon-2; gtl-1* mutants were counted based on a protruding-vulva phenotype.

Thrashing assays were performed as follows. A drop of M9 buffer was placed onto animals for examination on NGM assay plates, and then thrashes were counted for 20 s every 24 hr after the start of the assay.  $n = 3$  for each time point/strain.

### Nucleic acid analysis

Molecular biological methods were essentially as described (Ausubel, 1987; Sambrook et al., 1989). Other details are described in Supplemental Data.

### Assays using intestinal culture and a Ni<sup>2+</sup>-sensitive fluorescence indicator

Decapitation of each animal was performed in the following dissection solution: 136 mM NaCl, 9 mM KCl, 1 mM CaCl<sub>2</sub>, 3 mM MgCl<sub>2</sub>, 24 mM glucose, and 5 mM HEPES (pH 7.4). The dissected intestine was incubated in dissection solution at room temperature, and the intestine was treated with 0.2% pluronic acid F-127 and 20  $\mu$ M calcein AM for 30 min. After incubation, the specimens were washed with dissection solution three times, and the intestinal cells that were connected to the anterior part of the body were cut out. Then, the specimens were set onto the fluorescence microscope. The specimens were always perfused with the dissection solution containing either 0, 0.01, 0.1, or 1 mM NiCl<sub>2</sub> as described in Figure 5. In the first 100–300 s, the specimens were perfused with 0 mM NiCl<sub>2</sub>, and the slope during this period was used to normalize a quenching rate without NiCl<sub>2</sub> for calcein fluorescence.

Optical recordings were performed on a Zeiss Axioskop 2 upright compound microscope fitted with a Hamamatsu Orca ER CCD camera, a Uni-blitz Shutter Unit. Fluorescence images were acquired and saved using Metafluor Software (Universal Imaging, Inc.). Samples were taken every 20 s (a 10 millisecond exposure time with a 4  $\times$  4 binning) using a 40 $\times$  Zeiss Water-Immersion objective. FITC Filter/dichroic pairs and a neutral density filter (5%) were used (Chroma). Normalization and analyses were performed using Igor Pro 4.07 (Wavemetrics, Inc).

### Electrophysiology of cell culture

All strains were kept on 40 mM Mg<sup>2+</sup> NGM lite plates at 20°C. Embryonic cells were prepared as described (Christensen et al., 2002). Cells were kept at 24°C–25°C until used. As described, the intestinal cells were identified by their distinct round morphology containing autofluorescent granules (Estevez et al., 2003).

Patch clamp recordings were performed as follows (Estevez et al., 2003). The pipette solution contained 147 mM NaGluconate, 0.6 mM CaCl<sub>2</sub>, 1 mM MgCl<sub>2</sub>, 10 mM EGTA, 10 mM HEPES, 2 mM NaATP, and 0.5 mM Na2GTP (340 mOsm with sucrose), and its pH was adjusted with CsOH to 7.2. EGTA (10 mM) was replaced with 10 mM BAPTA when noted. The bath solution contained 145 mM NaCl, 1 mM CaCl<sub>2</sub>, 5 mM MgCl<sub>2</sub>, 10 mM HEPES, and 20 mM glucose (pH 7.2 with NaOH and 340 mOsm with sucrose). For solution replacement assays, the following solutions were used: 150 mM NaCl solution, 150 mM NaCl, 1 mM NMDG, 1 mM HEPES, 20 mM glucose, 1 mM EDTA (pH 7.2) adjusted by HCl, 340–345 mOsm. All other solutions contained 1 mM HEPES and 20 mM glucose and were also adjusted pH at 7.2 by HCl and 340–345 mOsm (120 mM MgCl<sub>2</sub> solution: 120 mM MgCl<sub>2</sub>, 1 mM NMDG; 120 mM CaCl<sub>2</sub> solution: 120 mM CaCl<sub>2</sub>, 1 mM NMDG; 5 mM NiCl<sub>2</sub> solution: 5 mM NiCl<sub>2</sub>, 130 mM NMDG; 150 mM NMDG solution: 150 mM NMDG). Solutions were perfused using the Warner SF-77B Perfusion system. Liquid junction potentials were measured as previously described (Neher, 1992).

Whole-cell currents were recorded using a Multiclamp700A and pClamp 8.2 and were analyzed using Clampfit 8.2 (Axon Instruments). Electrodes were fabricated from borosilicate glass capillaries (World Precision Instruments, 1B120F-4) and pressure polished as described

(Goodman and Lockery, 2000). Typical electrode resistances were ~10 M $\Omega$  after pressure polishing. To estimate the Mg<sup>2+</sup> dose response of the outwardly rectifying current, intracellular free Mg<sup>2+</sup> was estimated by WEBMAXC (<http://www.stanford.edu/~cpatton/webmaxc/>), and K<sub>1/2</sub> values of intracellular [Mg<sup>2+</sup>] were calculated by fitting one-phase exponential decay curves using Prism 4.0 (GraphPad Software, Inc.). The permeability of NMDG<sup>+</sup> relative to Na<sup>+</sup> was calculated by the equation  $P_{\text{NMDG}^+}/P_{\text{Na}^+} = ([\text{NMDG}^+]_o/[\text{Na}^+]_o) \exp(\Delta E_{\text{rev}}F/RT)$  (Hille, 1991).

### Trace element assay

N2 and *gon-2 gtl-1* mutant animals were grown at 15°C on 40 mM Mg<sup>2+</sup> plates, then rinsed off with water and transferred to NGM-lite (0 mM Mg<sup>2+</sup>) plates at 23.5°C. After ~24 hr of incubation, worms were rinsed off plates with water, washed twice with water to remove *E. coli*, and then pelleted in microfuge tubes. The dry weight of each pellet was determined by pre-weighing the tube, then drying down the worms in a speed vac oven under medium heat for 2 hr and reweighing the tube. Worm pellets were dissolved in concentrated nitric acid, appropriate dilutions were made with ultrapure water, and the samples were analyzed with a collision/reaction cell inductively coupled plasma mass spectrometer (ICP-MS, Agilent 7500 Octopole Reaction System). Spectral interferences were removed by pressurizing the octopole collision cell with H<sub>2</sub> (Ca, Zn, Fe) or He (Mg, K, Cu).

### Supplementary Material

Refer to Web version on PubMed Central for supplementary material.

### Acknowledgements

We thank K. Bray, R. Toyonaga, and K. Sakaguchi for technical assistance; H. Inada and I. Mori for a knockout library; the *C. elegans* gene Knockout Consortium for the *gtl-1(ok375)* strain; the *C. elegans* Genome Project Consortium for cosmids; A. Fire for GFP vectors; Y. Kohara for yk cDNA clones; S. Sturup for the ICP-MS analysis; J. Surmeier for an osmometer; and S. DeVries, K. Nagata, and M. Doi for discussion. This work was supported by funds from Northwestern University (to K.I.) and NIH R01GM49785 (to E.J.L.). K.I. is a Kyakuin-Kenkyuin Scientist of AIST. Some strains were obtained from the Caenorhabditis Genetics Center, which is funded by the National Institutes of Health, National Center for Research Resources of the U.S. This paper is dedicated to the late Professor Tadashi Ishimoda-Takagi.

### References

- Aronson, PS.; Boron, WF.; Boulpaep, EL. Physiology of membranes. In: Boron, WF.; Boulpaep, EL., editors. Medical Physiology: A Cellular and Molecular Approach. Philadelphia: Saunders Publishing; 2003. p. 50-86.
- Ausubel, FM. Current Protocols in Molecular Biology. New York: John Wiley & Sons, Inc.; 1987.
- Birnbaumer L, Yidirim E, Abramowitz J. A comparison of the genes coding for canonical TRP channels and their M, V and P relatives. Cell Calcium 2003;33:419–432. [PubMed: 12765687]
- Cabantchik ZI, Glickstein H, Milgram P, Breuer W. A fluorescence assay for assessing chelation of intracellular iron in a membrane model system and in mammalian cells. Anal Biochem 1996;233:221–227. [PubMed: 8789722]
- Christensen M, Estevez A, Yin X, Fox R, Morrison R, McDonnell M, Gleason C, Miller DM 3rd, Strange K. A primary culture system for functional analysis of *C. elegans* neurons and muscle cells. Neuron 2002;33:503–514. [PubMed: 11856526]
- Chubanov V, Waldegger S, Mederos y Schnitzler M, Vitzthum H, Sassen MC, Seyberth HW, Konrad M, Gudermann T. Disruption of TRPM6/TRPM7 complex formation by a mutation in the TRPM6 gene causes hypomagnesemia with secondary hypocalcemia. Proc Natl Acad Sci USA 2004;101:2894–2899. [PubMed: 14976260]
- Clapham DE. TRP channels as cellular sensors. Nature 2003;426:517–524. [PubMed: 14654832]

- Dal Santo P, Logan MA, Chisholm AD, Jorgensen EM. The inositol trisphosphate receptor regulates a 50-second behavioral rhythm in *C. elegans*. *Cell* 1999;98:757–767. [PubMed: 10499793]
- Epstein, HF.; Shakes, DC. *Caenorhabditis elegans: Modern Biological Analysis of an Organism*. San Diego, CA: Academic Press, Inc; 1995.
- Estevez AY, Roberts RK, Strange K. Identification of store-independent and store-operated Ca<sup>2+</sup> conductances in *Caenorhabditis elegans* intestinal epithelial cells. *J Gen Physiol* 2003;122:207–223. [PubMed: 12860924]
- Flatman PW. Mechanisms of magnesium transport. *Annu Rev Physiol* 1991;53:259–271. [PubMed: 2042962]
- Fox C, Ramsomair D, Carter C. Magnesium: its proven and potential clinical significance. *South Med J* 2001;94:1195–1201. [PubMed: 11811859]
- Goodman MB, Lockery SR. Pressure polishing: a method for re-shaping patch pipettes during fire polishing. *J Neurosci Methods* 2000;100:13–15. [PubMed: 11040361]
- Grimm C, Kraft R, Sauerbruch S, Schultz G, Harteneck C. Molecular and functional characterization of the melastatin-related cation channel TRPM3. *J Biol Chem* 2003;278:21493–21501. [PubMed: 12672799]
- Harteneck C, Plant TD, Schultz G. From worm to man: three subfamilies of TRP channels. *Trends Neurosci* 2000;23:159–166. [PubMed: 10717675]
- Hille, B. *Ionic Channels of Excitable Membranes*. Sunderland, MA: Sinauer Associates Inc.; 1991.
- Hofmann T, Chubakov V, Gudermann T, Montell C. TRPM5 is a voltage-modulated and Ca<sup>2+</sup>-activated monovalent selective cation channel. *Curr Biol* 2003;13:1153–1158. [PubMed: 12842017]
- Jansen G, Hazendonk E, Thijssen KL, Plasterk RH. Reverse genetics by chemical mutagenesis in *Caenorhabditis elegans*. *Nat Genet* 1997;17:119–121. [PubMed: 9288111]
- Jusofie A, Kirsch M, de Groot H. Ca<sup>2+</sup>-dependent cytotoxicity of H<sub>2</sub>O<sub>2</sub> in L929 cells: the role of H<sub>2</sub>O<sub>2</sub>-induced Na<sup>+</sup>-influx. *Free Radic Biol Med* 1998;25:712–719. [PubMed: 9801072]
- Liu DW, Thomas JH. Regulation of a periodic motor program in *C. elegans*. *J Neurosci* 1994;14:1953–1962. [PubMed: 8158250]
- Minke B, Cook B. TRP channel proteins and signal transduction. *Physiol Rev* 2002;82:429–472. [PubMed: 11917094]
- Monteilh-Zoller MK, Hermosura MC, Nadler MJ, Scharenberg AM, Penner R, Fleig A. TRPM7 provides an ion channel mechanism for cellular entry of trace metal ions. *J Gen Physiol* 2003;121:49–60. [PubMed: 12508053]
- Montell C. Physiology, phylogeny, and functions of the TRP superfamily of cation channels. *Sci STKE* 2001 2001:RE1.
- Montell C. Mg<sup>2+</sup> Homeostasis: the Mg<sup>2+</sup>-sensitive TRPM channels. *Curr Biol* 2003a;13:R799–R801. [PubMed: 14561419]
- Montell C. The venerable invertebrate TRP channels. *Cell Calcium* 2003b;33:409–417. [PubMed: 12765686]
- Nadler MJ, Hermosura MC, Inabe K, Perraud AL, Zhu Q, Stokes AJ, Kurosaki T, Kinet JP, Penner R, Scharenberg AM, Fleig A. LTRPC7 is a Mg<sup>2+</sup>-ATP-regulated divalent cation channel required for cell viability. *Nature* 2001;411:590–595. [PubMed: 11385574]
- Neher E. Correction for liquid junction potentials in patch clamp experiments. *Methods Enzymol* 1992;207:123–131. [PubMed: 1528115]
- Nicotera P, Bano D. The enemy at the gates. Ca<sup>2+</sup> entry through TRPM7 channels and anoxic neuronal death. *Cell* 2003;115:768–770. [PubMed: 14697196]
- Peredney CL, Williams PL. Utility of *Caenorhabditis elegans* for assessing heavy metal contamination in artificial soil. *Arch Environ Contam Toxicol* 2000;39:113–118. [PubMed: 10790509]
- Romani AM, Scarpa A. Regulation of cellular magnesium. *Front Biosci* 2000;5:D720–D734. [PubMed: 10922296]
- Runnels LW, Yue L, Clapham DE. TRP-PLIK, a bifunctional protein with kinase and ion channel activities. *Science* 2001;291:1043–1047. [PubMed: 11161216]
- Saitou N, Nei M. The neighbor-joining method: a new method for reconstructing phylogenetic trees. *Mol Biol Evol* 1987;4:406–425. [PubMed: 3447015]

- Sambrook, J.; Fritsch, EF.; Maniatis, T. *Molecular Cloning, A Laboratory Manual*. 2. Cold Spring Harbor, NY: Cold Spring Harbor Laboratory Press; 1989.
- Schlingmann KP, Weber S, Peters M, Niemann Nejsum L, Vitzthum H, Klingel K, Kratz M, Haddad E, Ristoff E, Dinour D, et al. Hypomagnesemia with secondary hypocalcemia is caused by mutations in TRPM6, a new member of the TRPM gene family. *Nat Genet* 2002;31:166–170. [PubMed: 12032568]
- Schmitz C, Perraud AL, Johnson CO, Inabe K, Smith MK, Penner R, Kurosaki T, Fleig A, Scharenberg AM. Regulation of vertebrate cellular Mg<sup>2+</sup> homeostasis by TRPM7. *Cell* 2003;114:191–200. [PubMed: 12887921]
- Sun AY, Lambie EJ. gon-2, a gene required for gonadogenesis in *Caenorhabditis elegans*. *Genetics* 1997;147:1077–1089. [PubMed: 9383054]
- Thomas JH. Genetic analysis of defecation in *Caenorhabditis elegans*. *Genetics* 1990;124:855–872. [PubMed: 2323555]
- Voets T, Nilius B, Hoefs S, van der Kemp AW, Droogmans G, Bindels RJ, Hoenderop JG. TRPM6 forms the Mg<sup>2+</sup> influx channel involved in intestinal and renal Mg<sup>2+</sup> absorption. *J Biol Chem* 2004;279:19–25. [PubMed: 14576148]
- Vormann J. Magnesium: nutrition and metabolism. *Mol Aspects Med* 2003;24:27–37. [PubMed: 12537987]
- Walder RY, Landau D, Meyer P, Shalev H, Tsoia M, Borochowitz Z, Boettger MB, Beck GE, Englehardt RK, Carmi R, Sheffield VC. Mutation of TRPM6 causes familial hypomagnesemia with secondary hypocalcemia. *Nat Genet* 2002;31:171–174. [PubMed: 12032570]
- West RJ, Sun AY, Church DL, Lambie EJ. The *C. elegans* gon-2 gene encodes a putative TRP cation channel protein required for mitotic cell cycle progression. *Gene* 2001;266:103–110. [PubMed: 11290424]
- White, J. The anatomy. In: Williams, BW., editor. *The Nematode Caenorhabditis elegans*. Cold Spring Harbor, NY: Cold Spring Harbor Laboratory; 1987. p. 81-122.
- Wolf FI. TRPM7: channeling the future of cellular magnesium homeostasis? *Sci STKE* 2004 2004:pe23.



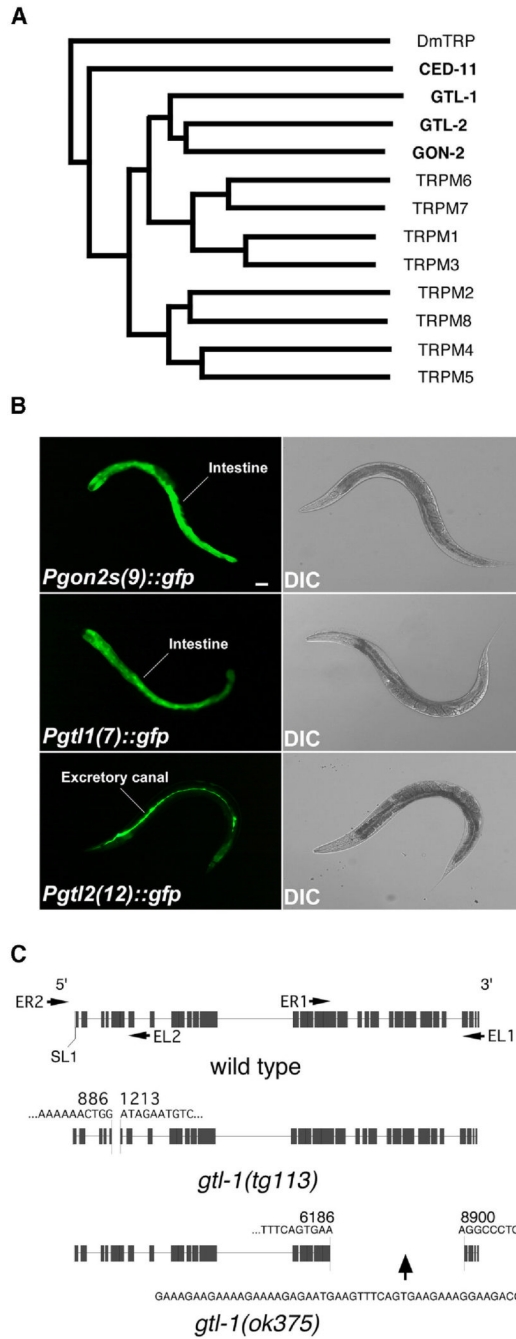


**Figure 1. TRPM channels in *C. elegans***

**A)** A phylogenetic tree of *C. elegans*, *Drosophila*, and human TRPM proteins. DmTRP indicates the TRP channel of *D. melanogaster*. CED-11, GTL-1, GTL-2, and GON-2 are *C. elegans* TRPMs. TRPM 1–8 are human proteins. Relationships were inferred by the Neighbor-Joining Method (Saitou and Nei, 1987).

**B)** Expression of *gon-2*, *gtl-1*, and *gtl-2*. *Pgon2s(9)::gfp* and *Pgtl1(7)::gfp* fusion genes were strongly expressed in the intestine. Bar, 50  $\mu$ .

**C)** Characterization of *gtl-1* deletion mutants *tg113* and *ok375*. (Top) The structure of the wild-type *gtl-1* gene and two pairs of PCR primers (ER1 and EL1, and ER2 and EL2). (Middle) The deleted region of *tg113*. (Bottom) The deleted region of *ok375* (a 50 nucleotide insertion was

found at the junction). All numbers shown at the junction sites are the numbers of nucleotides starting from the first ATG initiation codon.

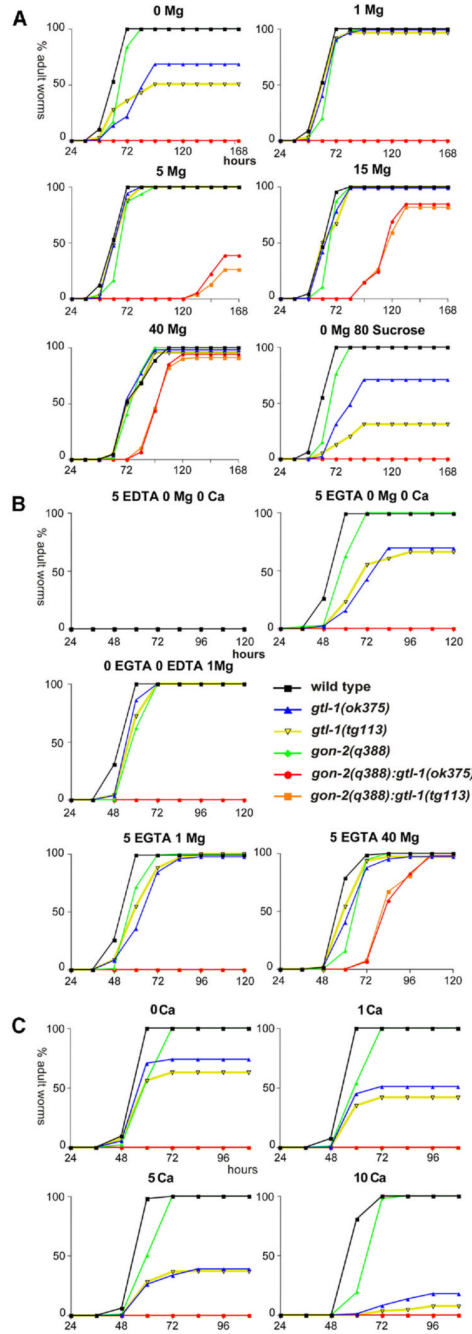


**Figure 2. Growth of mutants at different  $Mg^{2+}/Ca^{2+}$  concentrations**

**A)** Growth of mutants at different  $Mg^{2+}$  concentrations. Strains were maintained on NGM agar plates containing 40 mM  $Mg^{2+}$  and 0 mM  $Ca^{2+}$  for at least three generations at 20°C. Fifty eggs were picked for each strain and placed on a fresh plate containing different  $Mg^{2+}$  concentrations. All animals were grown at 25°C during the assays. The mean of two independent assays is plotted.

**B)** Growth of mutants at different EDTA and EGTA concentrations. No  $Ca^{2+}$  or  $Mg^{2+}$  was added unless noted. For details, see above.

**C)** Effects of  $Ca^{2+}$  on growth. No  $Mg^{2+}$  was added in the agar.

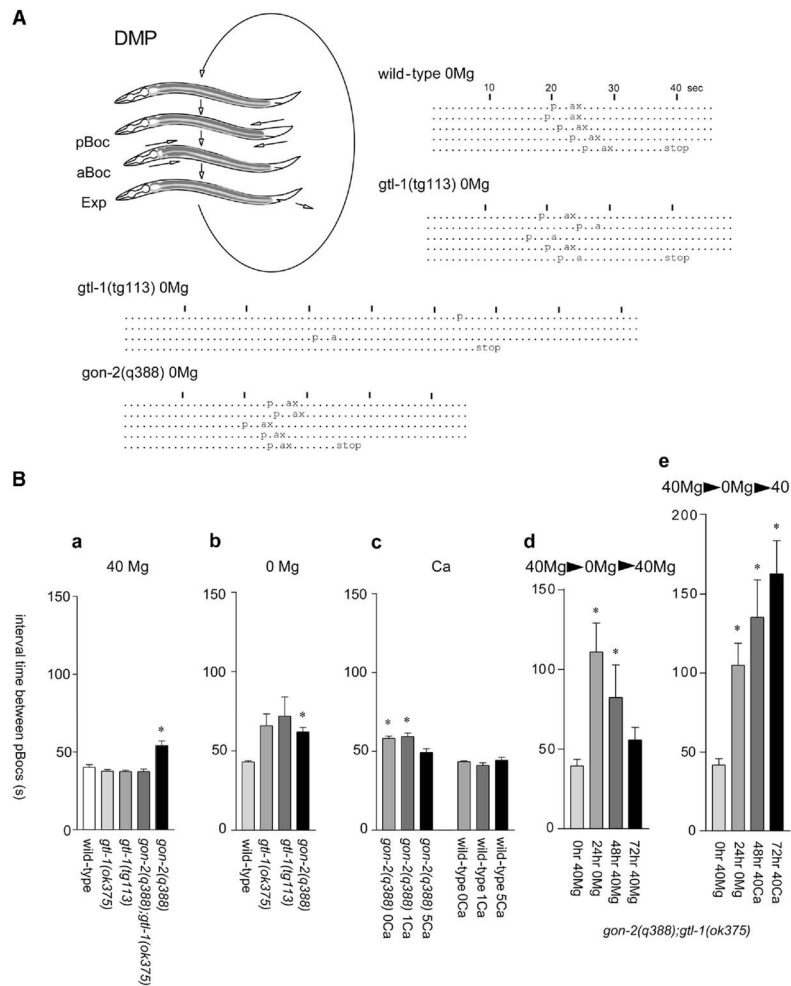


### Figure 3. The defecation motor program

**A)** Schematic representation of the defecation motor program (DMP) and representative ethograms of defecation behavior. (1) Intercycle (not labeled); (2) pBoc, posterior body wall muscle contraction; (3) aBoc, anterior body wall muscle contraction; (4) Exp, enteric muscle contraction with expulsion of gut contents, then return to the intercycle. In ethograms, each dot or character represents 1 s. Seconds elapsed are indicated above each ethogram. p, a, and x represent pBoc, aBoc, and Exp, respectively. The mean defecation cycle was  $43.0 \pm 1.5$  (standard deviation) for a wild-type at 0 mM  $Mg^{2+}$ . Forty percent of *gtl-1(tg113)* mutants at 0 mM  $Mg^{2+}$  showed near-normal cycles, while 60% of them showed longer cycles. *gon-2(q388)* at 0 mM  $Mg^{2+}$  showed a  $62.0 \pm 6.4$  s cycle.

**B)** Effects of  $Mg^{2+}$  and  $Ca^{2+}$  concentrations on the defecation behavior. All data were a summary of five cycles/animal from at least five animals for each strain. All strains were grown at 25°C. \* $p < 0.05$  (Mann-Whitney test). **(Ba)** The DMP cycles on 40 mM  $Mg^{2+}$  plates.  $Ca^{2+}$  was not added to the plates. **(Bb)** The DMP cycles on 0 mM  $Mg^{2+}$  plates. The DMP cycles of the *gtl-1* mutants were affected, but this phenotype varied largely from individual to individual. Although mean DMP cycles were substantially longer, some individuals showed the nearly wild-type DMP cycles (see the second example in [A]). **(Bc)** Effects of  $Ca^{2+}$  concentrations on the defecation behavior. The DMP cycles were measured on NGM agar plates containing different  $Ca^{2+}$  concentrations.  $Mg^{2+}$  was not included in these plates. **(Bd)** DMP assays with the *gon-2(q388);gtl-1(ok375)* double mutant. Since the double mutants did

not grow on 0 mM Mg<sup>2+</sup> plates, they were grown on 40 mM Mg<sup>2+</sup> plates until they were L3 larvae and then transferred to 0 mM Mg<sup>2+</sup> plates. The same animals were transferred back to 40 mM Mg<sup>2+</sup> plates at the 70th hour from the beginning of the assay. Wild-type animals that were tested in parallel were not affected by the first plate transfer. However, these wild-type animals became too old during the assay while the double mutants arrested on 0 mM Mg<sup>2+</sup> plates. **(Be)** DMP defects in the *gon-2(q388);gtl-1(ok375)* double mutant were not rescued by excess Ca<sup>2+</sup>. The double mutants were grown on 40 mM Mg<sup>2+</sup> plates until they were L3 larvae and then transferred to 0 mM Mg<sup>2+</sup> plates. The same animals were transferred back to 40 mM Ca<sup>2+</sup> plates at the 70th hour from the beginning of the assay.



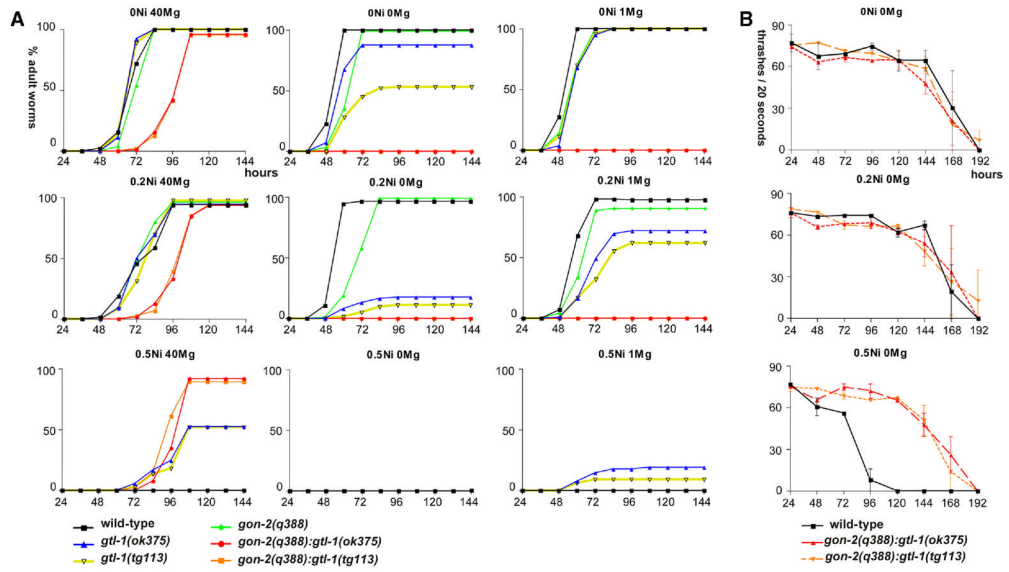


**Figure 4. Effects of Ni<sup>2+</sup> on animal growth**

**A)** Ni<sup>2+</sup> toxicity assays. Fifty eggs were picked for each strain and placed on fresh plates containing different Ni<sup>2+</sup> and Mg<sup>2+</sup> concentrations. See Figure 2 for details. The *gon-2;gtl-1* mutants showed resistance to Ni<sup>2+</sup> toxicity. The *gtl-1* mutants acquired resistance to toxicity in a Mg<sup>2+</sup>-dependent manner.

**B)** Viability of the *gon-2;gtl-1*-double mutants on 0 mM Mg<sup>2+</sup> plates containing different Ni<sup>2+</sup> concentrations. The resistance of the double mutants to 0.5 mM Ni<sup>2+</sup> was examined using a thrashing assay, counting the number of times the animal swung from side to side in a saline solution. The x axis indicates the time (hr) elapsed after the start of the assay, and the y axis indicates the number of thrashes per 20 s interval. n = 3 for each time point/strain. Error bars indicate standard errors.

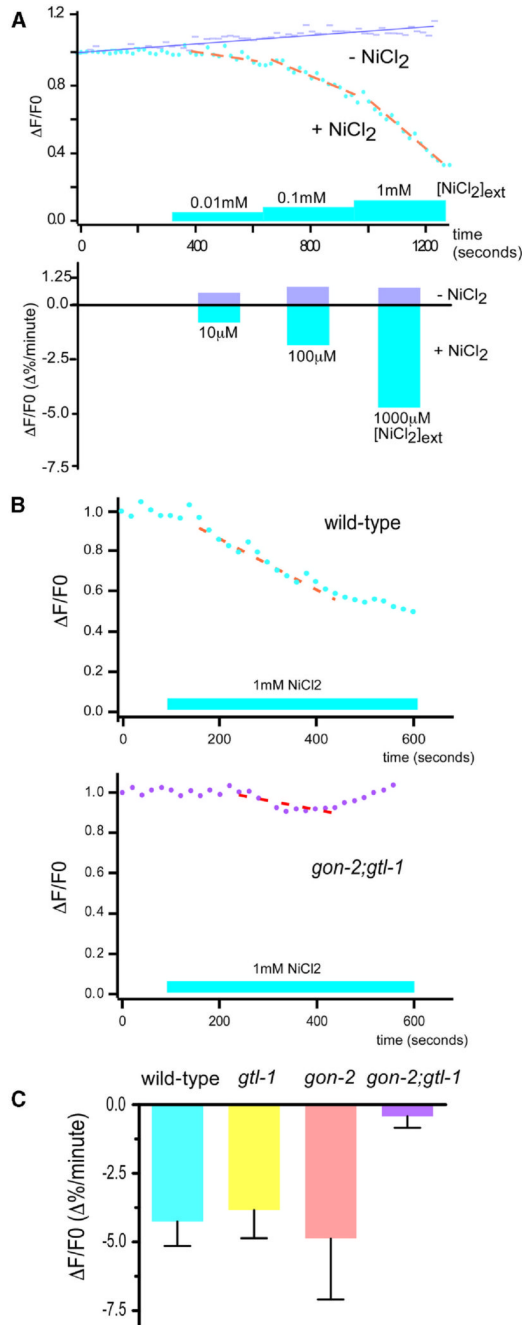


**Figure 5. Detection of Ni<sup>2+</sup> absorption in dissected intestine preparations**

**A)** Fluorescence of the Ni<sup>2+</sup> indicator calcein reflects Ni<sup>2+</sup> absorption by dissected intestine. Dissected intestine loaded with 20  $\mu$ M calcein was perfused with the dissection solution for 300 s, followed by the solution with different Ni<sup>2+</sup> concentrations. “ $\Delta F/F_0$ ” indicates fluorescence intensity normalized by the intensity at time 0 (F<sub>0</sub>). The x axis is the time elapsed (s). “ $\Delta F/F_0$  ( $\Delta\%/minute$ )” indicates the percent of fluorescence quenching per minute. The higher the Ni<sup>2+</sup> concentration, the faster the calcein fluorescence quenched (n = 3, labeled “+NiCl<sub>2</sub>”). Calcein fluorescence did not significantly decrease without Ni<sup>2+</sup> perfusion (n = 6, labeled “-NiCl<sub>2</sub>”). The nonspecific fluorescence bleach was normalized using the first 300 s measurements for both slopes.

**B)** Quenching of calcein fluorescence by  $\text{Ni}^{2+}$  absorption. Details are same as above. The nonspecific fluorescence bleach was normalized using the first 100 s measurement. The *gon-2;glt-1* mutant ( $-1.9\% \pm 0.9\%/min$ ) showed a lower quenching rate than wild-type ( $-5.1 \pm 1.1$ );  $p < 0.05$  ( $n = 5-6$ ). Animals were grown on 40 mM  $\text{Mg}^{2+}$  plates.

**C)** Means and standard errors of the intestinal  $\text{Ni}^{2+}$  absorption in different strains.  $\text{Ni}^{2+}$  absorption was reduced in the intestine of the *gon-2;glt-1*-double mutant compared to other strains ( $p < 0.05$ ): wild-type,  $-4.2 \pm 0.9\%/min$ ; *glt-1(ok375)*,  $-3.8 \pm 1.0$ ; *gon-2(q388)*,  $-4.8 \pm 2.2$ ; *gon-2;glt-1*,  $-0.42 \pm 0.4$  ( $n = 5-17$ ). These animals were grown on NGM plates. The double mutant was grown on 40 mM  $\text{Mg}^{2+}$  plates and transferred to NGM plates at L3-L4 stages.

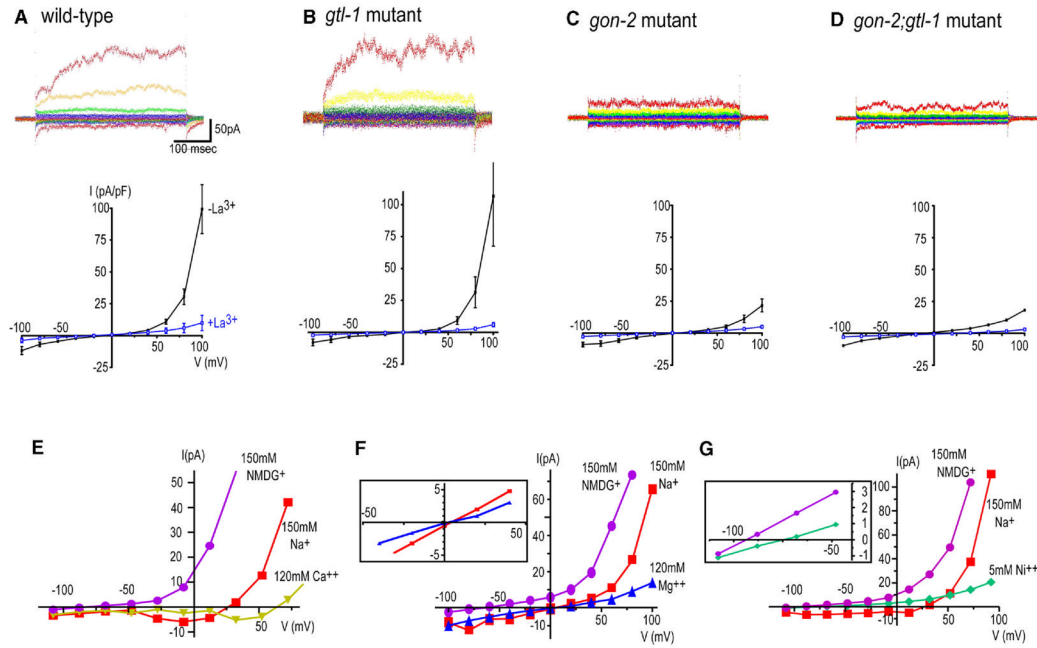


**Figure 6. Whole-cell currents in cultured intestinal cells**

**A–D)** Representative whole-cell currents. Currents were recorded by stepping from a holding voltage of 0 mV to voltages between –100 and +100 mV in 20 mV intervals. (Middle panels) Steady-state I–V relationship for whole-cell currents (n = 4–9 each, the bars are standard errors). This current was suppressed in the presence of 0.1 mM LaCl<sub>3</sub> in the bath solution (n = 3–8 each).

**E)** I–V relationships of whole-cell current of the wild-type cells in the 150 mM Na<sup>+</sup> solution and when Na<sup>+</sup> was replaced with 120 mM Ca<sup>2+</sup>, then with 150 mM NMDG<sup>+</sup>. In the Na<sup>+</sup> solution, 1 mM EDTA was included to chelate residual divalent cations. Note that the current amplitude (the y axis) is not normalized with the membrane capacitance.

**F)** I–V relationships in 150 mM Na<sup>+</sup>, replaced with 120 mM Mg<sup>2+</sup>, then with 150 mM NMDG<sup>+</sup>. (Inset) A magnification of reversal potential points.

**G)** I–V relationships in 150 mM Na<sup>+</sup>, replaced with 5 mM Ni<sup>2+</sup> and 130 mM NMDG<sup>+</sup>, then with 150 mM NMDG<sup>+</sup>. (Inset) A magnification of reversal potential points for the Ni<sup>2+</sup> and NMDG<sup>+</sup> solutions.

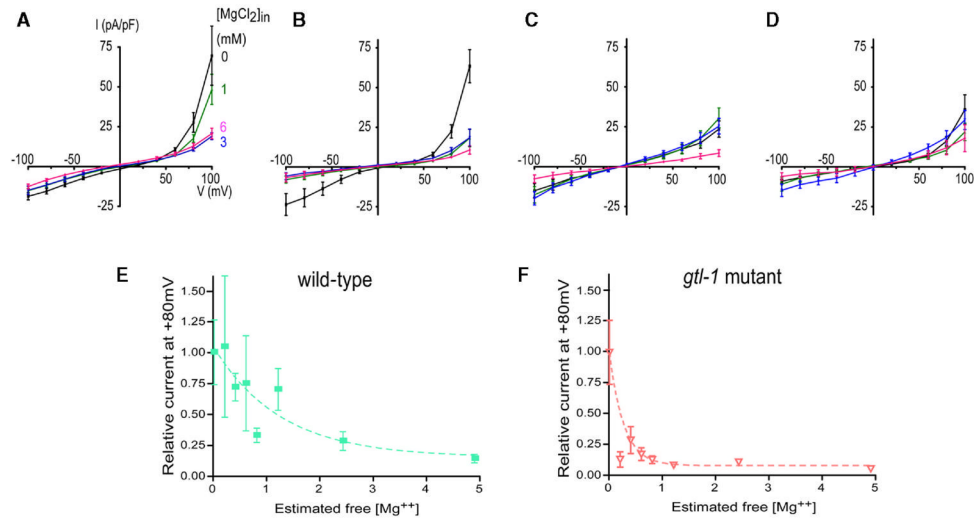


**Figure 7. Dose response relationship for inhibition of the outwardly rectifying current by intracellular free  $Mg^{2+}$**

**A)** Inhibition of current by intracellular  $Mg^{2+}$  in wild-type ( $n = 8-15$ ). The pipette solutions contained 0–6 mM  $MgCl_2$ . The protocol was essentially same as experiments in Figure 6.

**B)** *gtl-1(ok375)* mutant cells;  $n = 4-8$ .

**C)** *gon-2(q388)* mutant cells;  $n = 5-10$ .

**D)** *gon-2(q388);gtl-1(ok375)* double mutant cells;  $n = 4-8$ .

**E and F)** Currents were recorded by stepping from a holding voltage of 0 mV to voltages between  $-100$  and  $+100$  mV in 20 mV intervals, and the amplitudes of steady-state current at  $+80$  mV were normalized based on the mean amplitude at  $+80$  mV of 0 mM  $Mg^{2+}$  added in the pipette solution. The y axis is this normalized current amplitude, and the x axis is intracellular free  $Mg^{2+}$  levels estimated by WEBMAXC program. The pipette solutions contained 0–6 mM  $MgCl_2$  with no ATP and GTP, and with 10 mM BAPTA instead of EGTA.  $K_{1/2}$  values were 874  $\mu M$  for wild-type ([E],  $n = 4$  each point) and 186 for the *gtl-1* mutant ([F],  $n = 3-7$ ). All results presented in this figure were obtained independently of the experiments in Figure 6.